

**Fig. 2:** Measured optical spectra at 0.03-nm resolution: (a) the baseband optical signals of dual-channels after OTU; (b) the optical signals and optical LO after optical coupler; (c) remodulation optical signals without and with filtering.

channel transparent fiber-THz-fiber  $2 \times 2$  MIMO transmission system based on optical-to-THz (O/T) and THz-to-optical (T/O) conversion is shown in Fig. 1. Four CFP2-DCO modules are used for optical baseband signals real-time processing. The double-carrier frequency of channel 1 (Ch1) and channel 2 (Ch2) is fixed at 193.5 THz and 193.55 THz with 3 dBm output optical power, respectively. The frequency space between Ch1 and Ch2 meet 50 GHz ITU-T grid. Each CFP2-DCO module works at 100 GbE mode, and 31.379 GBaud DP-QPSK modulated optical baseband signal with a roll-off factor of 0.2 is generated. The optical spectrum of the coupled Ch1 and Ch2 is shown in Fig. 2(a).

At the O/T converter, over 20 km SSF, the optical signals with 10.6 dBm optical power and the ECL-1 with 13.5 dBm optical power operating at 193.115 THz as an optical local oscillator (LO) are coupled, and then amplified by an EDFA to effectively drive antenna-integrated photomixer modules (AIPMs) based on uni-travelling-carrier photodiode (UTC-PD). The optical spectrum of the coupled optical signals and optical LO are shown in Fig. 3(b). The frequency space between Ch1, Ch2 and LO is fixed at 385 GHz and 435 GHz, respectively. A polarization beam splitter (PBS) is used to polarization diversity, and X- and Y-polarization components are up-converted by AIPMs to two THz-wave wireless signals at 385 GHz and 435 GHz corresponding to Ch1 and Ch2. The AIPMs are polarization sensitive, and two PCs are necessary to adjust the incident polarization direction to maximize output power from AIPMs. Then, the THz-wave signals are delivered over a 3 m  $2 \times 2$  MIMO wireless transmission link. Three pairs of lenses are used to focus the wireless THz-wave to maximize the received THz-wave signal power.

At the T/O converter, hybrid optoelectronic down-conversion is used for T/O conversion in order to reduce the carrier frequency and the bandwidth requirement for the modulators. For X- and Y-polarization THz-wave wireless signals, two identical THz receivers are driven by electronic LO sources to implement analog down

conversion, and each consists of a mixer, a  $\times 12$  frequency multiplier chain and an amplifier. The intermediate frequency (IF) signal bandwidth of THz receivers is 40 GHz. Note that, subject to the availability of the THz receivers, Ch1 and Ch2 is separately measured, but the total  $2 \times 100$  GbE line rate from transmitter is consistent all the time. The sinusoidal LO sources for Ch1 and Ch2 are set 30 GHz and 38.333 GHz, respectively. Hence the frequency of IF signals corresponding to Ch1 and Ch2 are same  $385 - 30 \times 12 = 25$  GHz and  $38.333 \times 12 - 435 = 25$  GHz. Then, the down-converted X- and Y-polarization IF signals at 25 GHz are boosted by electrical low-noise amplifiers (LNAs) to drive one integrated dual-polarization Mach-Zehnder Modulator (DP-MZM) with 3 dB bandwidth of 35 GHz and 1.8 V half-wave voltage, which operating at optical-carrier-suppression (OCS) point. Thus, four manual PCs are saved. The ECL-2 as the optical carrier input of the DP-MZM working at 193.525 THz, and the optical power after PM-EDFA is 19 dBm. Fig. 2(c) show the measured spectra of optical signals remodulation without and with filtering for Ch1 and Ch2, respectively. For Ch1, another TOF is set to filter out the lower sideband and the central optical carrier as well as the ASE noise, only leaving the upper sideband. Similarly, for Ch2, TOF is set to filter out the upper sideband and optical carrier, leaving the lower sideband. The

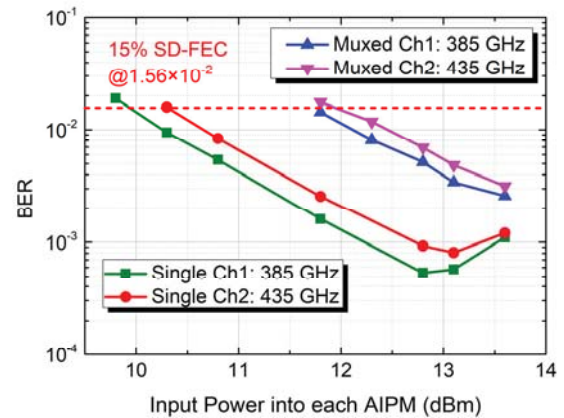


**Fig. 3:** BER versus input power into each AIPM for single channel case and dual-channel case.

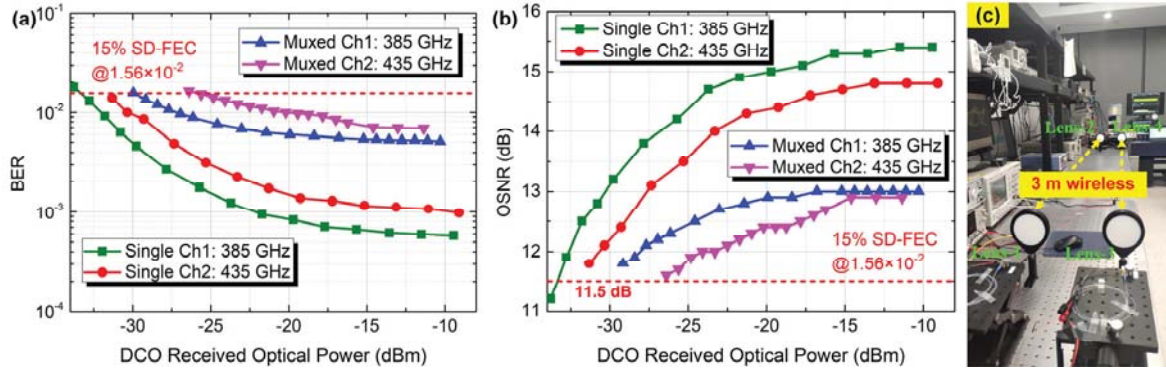


Fig. 4: (a) BER and (b) OSNR versus receive optical power (ROP) of each CFP2-DCO module for single channel case and dual-channel case at 385 GHz and 435 GHz, respectively. (c) Photo of 3 m wireless link.

obtained optical baseband signal is delivered over the second span of 20 km SSMF, and then received by CFP2-DCO modules corresponding to Ch1 or Ch2. A variable optical attenuator (VOA) is used to measure optical signal to noise ratio (OSNR) of the receiver. Figs. 2(a)-(c) are corresponding to the test points (i)-(iv) in Fig. 1.

## Results

The parameters, including operating mode, wavelength, output optical power, pre-BER and so on, can be set and monitored by the network management system (NMS). Each CFP2-DCO module can support 15% soft-decision forward-error-correction (SD-FEC) for pre-FEC BER of  $1.56 \times 10^{-2}$  and post-FEC BER  $< 10^{-15}$ . The dual-channel 31.379 GBaud (125.516 Gbps) DP-QPSK signals can provide  $2 \times 103.125$  Gbps net capacity for  $2 \times 100$  GbE clients.

Fig. 3 shows the BER versus the input power into each AIPM for single channel case and dual-channel case at 385 GHz and 435 GHz over two spans of 20 km SSMF and 3 m wireless distance, respectively. For single channel case, the BER performance begins to deteriorate over 13.1 dBm because the power of AIPMs are saturated. About 0.5 dB BER gain is achieved at 15% SD-FEC threshold for Ch1 at 385 GHz compared with Ch2 at 485 GHz. In order to avoid damaging AIPMs, the input optical power remains below 13.8 dBm in the dual-channel case. The BER performance of Ch1 and Ch2 is similar, and there is no power saturation phenomenon since dual-channel multiplexing reduce the average power of each channel. At 15% SD-FEC threshold, there are around 2 dB optical power penalty at 385 GHz and 435 GHz for dual-channel case compared with single channel case.

Then, we evaluate the BER and OSNR performance versus received optical power (ROP) of each CFP2-DCO module over two spans of 20 km SSMF and 3 m wireless distance link. Figs. 4(a) and (b) show the BER and OSNR versus ROP for single channel case and dual-channel

case at 385 GHz and 435 GHz, respectively. With increasing of ROP, BER and OSNR are gradually stable. In Fig. 4(a), we can observe that there are around 5 dB optical power penalty at 385 GHz and 435 GHz for dual-channel case compared with single channel case at 15% SD-FEC limit. In Fig. 4(b), the OSNR lower bound is around 11.5 dB corresponding to 15% SD-FEC threshold. Compared with single channel case, there are about 5 dB OSNR penalty at 385 GHz and 435 GHz for dual-channel case. Fig. 4(c) shows the photo of 3 m wireless link. This demonstrated fiber-THz-fiber seamless system can potentially support tens of users for bandwidth-consuming services, such as 3D holographic, metaverse, and 8K/10K video.

## Conclusions

A real-time dual-channel fiber-THz-fiber  $2 \times 2$  MIMO seamless transmission system with a record net data rate of  $2 \times 103.125$  Gbps under 15% SD-FEC is experimentally demonstrated at 385 GHz and 435 GHz THz band using the commercial DCO modules over two spans of 20 km SSMF and 3 m wireless link. O/T conversion at the transmitter is based on photomixing without THz power amplifier, T/O conversion at the receiver relies on hybrid optoelectronic down-conversion using commercial devices. One integrated DP-MZM and only two PCs are used to simplify the system. It's a promising scheme to meet the demands of future THz seamless integration for low power consumption, low cost and miniaturization. Photonics combined with electronic active devices may lever the THz wireless transmission distance for km-range.

## Acknowledgements

This work was partially supported by National Natural Science Foundation of China (62101121, 62101126), Major Key Project of PCL (PCL2021A01-2), China Postdoctoral Science Foundation (2021M702501), and Key Research and Development Program of Jiangsu Province (BE2020012).



## References

- [1] T. Nagatsuma, G. Ducournau, and C. C. Renaud, "Advances in terahertz communications accelerated by photonics," *Nat. Photonics* 10, 371-379 (2016). DOI: <https://doi.org/10.1038/nphoton.2016.65>
- [2] T. Harter, S. Ummethala, M. Blaicher, S. Muehlbrandt, S. Wolf, M. Weber, M. M. H. Adib, J. N. Kemal, M. Merboldt, F. Boes, S. Nellen, A. Tessmann, M. Walther, B. Globisch, T. Zwick, W. Freude, S. Randel, and C. Koos, "Wireless THz link with optoelectronic transmitter and receiver," *Optica* 6, 1063-1070 (2019). DOI: <https://doi.org/10.1364/OPTICA.6.001063>
- [3] K. Sengupta, T. Nagatsuma, and D. M. Mittleman, "Terahertz integrated electronic and hybrid electronic-photonic systems," *Nat. Electron.* 1, 622-635 (2018). DOI: <https://doi.org/10.1038/s41928-018-0173-2>
- [4] S. Jia, M. C. Lo, L. Zhang, O. Ozolins, A. Udalovs, D. Kong, X. Pang, R. Guzman, X. Yu, S. Xiao, S. Popov, J. Chen, G. Carpintero, T. Morioka, H. Hu, and L. Oxenløwe, "Integrated dual-laser photonic chip for high-purity carrier generation enabling ultrafast terahertz wireless communications," *Nat Commun* 13, 1388 (2022). DOI: <https://doi.org/10.1038/s41467-022-29049-2>
- [5] J. Yu, "Photonics-assisted millimeter-wave wireless communication," *IEEE J. Quantum Electron.* 53, 1-17 (2017). DOI: 10.1109/JQE.2017.2765742
- [6] S. Ummethala, T. Harter, K. Koehnle, Z. Li, S. Muehlbrandt, Y. Kutuvantavida, J. Kemal, P. Marin-Palomo, J. Schaefer, A. Tessmann, S. K. Garlapati, A. Bacher, L. Hahn, M. Walther, T. Zwick, S. Randel, W. Freude, and C. Koos, "THz-to-Optical Conversion in Wireless Communications Using an Ultra-Broadband Plasmonic Modulator," *Nat. Photonics* 13, 519-524 (2019). DOI: <https://doi.org/10.1038/s41566-019-0475-6>
- [7] Y. Horst, T. Blatter, L. Kulmer, B. I. Bitachon, B. Baeuerle, M. Destraz, W. Heni, S. Koepfli, P. Habegger, M. Eppenberger, E. De Leo, C. Hoessbacher, D. L. Elder, S. Hammond, L. Johnson, Y. Fedoryshyn, Y. Salamin, M. Burla, and J. Leuthold, "Transparent Optical-THz-Optical Link Transmission over 5/115 m at 240/190 Gbit/s Enabled by Plasmonics," in *Optical Fiber Communication Conference (OFC) 2021*, paper F3C.1. DOI: <https://doi.org/10.1364/OFC.2021.F3C.1>
- [8] C. Castro, R. Elschner, T. Merkle, C. Schubert, and R. Freund, "100 Gb/s Real-Time Transmission over a THz Wireless Fiber Extender Using a Digital-Coherent Optical Modem," in *Optical Fiber Communication Conference (OFC) 2020*, paper M4I.2. DOI: <https://doi.org/10.1364/OFC.2020.M4I.2>
- [9] J. Zhang, M. Zhu, M. Lei, B. Hua, Y. Cai, Y. Zou, L. Tian, A. Li, Y. Huang, J. Yu, and X. You, "Demonstration of Real-time 125.516 Gbit/s Transparent Fiber-THz-Fiber Link Transmission at 360 GHz ~ 430 GHz based on Photonic Down-Conversion," in *Optical Fiber Communication Conference (OFC) 2022*, paper M3C.2. DOI: <https://doi.org/10.1364/OFC.2022.M3C.2>
- [10] J. Zhang, M. Zhu, M. Lei, B. Hua, Y. Cai, Y. Zou, L. Tian, A. Li, Y. Wang, Y. Huang, J. Yu, and X. You, "Real-time demonstration of 103.125-Gbps fiber-THz-fiber 2 × 2 MIMO transparent transmission at 360-430 GHz based on photonics," *Opt. Lett.* 47, 1214-1217 (2022). DOI: <https://doi.org/10.1364/OL.448064>